HHS Public Access

Author manuscript

Nat Med. Author manuscript; available in PMC 2016 April 13.

Published in final edited form as:

Nat Med. 2014 August ; 20(8): 954–960. doi:10.1038/nm.3618.

Micropillar arrays as a high-throughput screening platform for therapeutics in multiple sclerosis

Feng Mei[#1], **Stephen P J Fancy**[#1,2], **Yun-An A Shen**[1], **Jianqin Niu**[3], **Chao Zhao**[4], **Bryan Presley**[5], **Edna Miao**[1], **Seonok Lee**[1], **Sonia R Mayoral**[1], **Stephanie A Redmond**[1], **Ainhoa Etxeberria**[1], **Lan Xiao**[3], **Robin J M Franklin**[4], **Ari Green**[1], **Stephen L Hauser**[1], and **Jonah R Chan**[1]

[1]Department of Neurology and Program in Neuroscience, University of California, San Francisco, San Francisco, California, USA.

[2]Department of Pediatrics, University of California, San Francisco, San Francisco, California, USA.

[3]Department of Histology and Embryology, Chongqing Key Laboratory of Neurobiology, Third Military Medical University, Chongqing, China.

[4]Wellcome Trust Medical Research Council, Cambridge Stem Cell Institute and Department of Veterinary Medicine, University of Cambridge, Cambridge, UK.

[5]Trianja Technologies, Allen, Texas, USA.

[#] These authors contributed equally to this work.

Abstract

Functional screening for compounds that promote remyelination represents a major hurdle in the development of rational therapeutics for multiple sclerosis. Screening for remyelination is problematic, as myelination requires the presence of axons. Standard methods do not resolve cell-autonomous effects and are not suited for high-throughput formats. Here we describe a binary indicant for myelination using micropillar arrays (BIMA). Engineered with conical dimensions, micropillars permit resolution of the extent and length of membrane wrapping from a single two-dimensional image. Confocal imaging acquired from the base to the tip of the pillars allows for detection of concentric wrapping observed as ‘rings’ of myelin. The platform is formatted in 96-well plates, amenable to semiautomated random acquisition and automated detection and quantification. Upon screening 1,000 bioactive molecules, we identified a cluster of antimuscarinic compounds that enhance oligodendrocyte differentiation and remyelination. Our findings

Correspondence should be addressed to J.R.C. (jonah.chan@ucsf.edu)..

Note: Any Supplementary Information and Source Data files are available in the online version of the paper.

AUTHOR CONTRIBUTIONS

F.M., S.P.J.F., Y.-A.A.S., J.N., C.Z., E.M., S.L. and J.R.C. performed experiments. F.M., S.P.J.F., B.P., L.X., R.J.M.F., S.L.H. and J.R.C. provided reagents. F.M., S.P.J.F., S.R.M., S.A.R., A.E., R.J.M.F., A.G., S.L.H. and J.R.C. provided intellectual contributions. F.M., S.P.J.F. and J.R.C. analyzed the data and wrote the paper.

COMPETING FINANCIAL INTERESTS

The authors declare no competing financial interests.

demonstrate a new high-throughput screening platform for potential regenerative therapeutics in multiple sclerosis.

Loss of myelin in diseases such as multiple sclerosis results in the disruption of the nerve signal, damage to the axon and, finally, neurodegeneration. In order to effectively treat these devastating conditions, new methodologies and approaches to promote repair are required. Unlike many degenerative diseases of the central nervous system (CNS), the rationale for repair in multiple sclerosis is compelling and represents a realistic near-term goal. Remyelination occurs in multiple sclerosis, but it is limited to specific regions in the CNS and becomes less efficient over time, ultimately resulting in axonal degeneration, a chronic process that appears to underlie disability in the progressive forms of the disease[1]. In the adult brain, oligodendrocytes are terminally differentiated and generally do not participate in repair[2]. Rather, remyelination is mediated by oligodendrocyte precursor cells (OPCs), which are present throughout the CNS and are rapidly mobilized to demyelinated lesions[3–6]. It is generally accepted that remyelination by adult OPCs is not hampered solely by issues of access or recruitment. Although adult OPCs may divide more slowly than their developmental counterparts[7–10], mitogens can augment proliferation of OPCs; however, they do not enhance remyelination in an aged mouse model[11]. This underscores the fact that a failure of OPC differentiation and membrane wrapping, rather than recruitment or migration of OPCs, is the critical barrier impeding myelin repair.

It has long been thought that the underlying mechanisms for oligodendrocyte differentiation and myelination are directly coupled to axonal signaling[12–16]. Recent findings have led to an alternative hypothesis suggesting that oligodendroglia have the capacity to myelinate paraformaldehyde-fixed axons[17] and even electron-spun nanofibers[18,19]. These findings suggest that pseudoaxonal substrates are sufficient to initiate concentric wrapping by oligodendrocytes and provide a minimally permissive environment ideally suited for analyzing cell-autonomous mechanisms necessary and sufficient for modeling myelination. Although the nanofiber scaffold represents a major advance for screening compounds, the fibers are not suitable for high-throughput screening. Spinning and patterning the nanofibers reproducibly into microwells can be accomplished only with great difficulty and is extremely time consuming. Additionally, automated detection and quantification of myelin internodes is not currently feasible, as there are various confounding issues associated with the varying lengths of myelin internodes and spatially overlapping oligodendroglial processes and cell bodies. To date, there are no therapies for oligodendrocyte remyelination, and this fact alone illustrates a great unmet need in the development of methodologies and approaches for regeneration and repair. Functional screening for small bioactive molecules that promote oligodendrocyte survival, differentiation and remyelination represents a major hurdle to the identification and development of rational therapeutics. Technical advances in the development of high-throughput screening platforms are needed to clarify the cell-autonomous mechanisms responsible for differentiation and remyelination. In this Technical Report, we outline the criteria for and conception of a high-throughput screening platform for myelination, introduce the fabrication of micropillar arrays and present findings arising from the completion of a 1,000-compound library screen. We report the identification of a cluster of US Food and Drug Administration (FDA)-approved antimuscarinic compounds

that greatly enhance oligodendrocyte differentiation and remyelination both *in vitro* and *in vivo*. Our findings and technical advances with new *in vitro* systems provide us with a unique opportunity to screen for and identify promising therapeutics for remyelination and repair in MS.

RESULTS

Fabrication of micropillar arrays for modeling myelination

We developed an approach that combines two innovative advances that together provide a platform for high-throughput screening, which we termed BIMA. We conceived the rationale for this approach after an in-depth examination of compressed *z*-stack images of oligodendrocytes wrapping nanofibers as previously described[18,19] (Fig. 1a). Upon examination of the side view of the myelin-like segments, we observed distinct myelin basic protein (MBP)-positive rings (Fig. 1b). The rings represent a binary indicant for concentric membrane wrapping by oligodendrocytes. Therefore, we fabricated micropillar arrays of compressed silica into a 96-well format for a more efficient and rapid experimental design (Fig. 1c,d). Essentially, micropillars represent freestanding nanofibers around which membrane wrapping can be visualized in cross-section, a feature that will allow for the detection of 'rings' of myelin membrane. Conceptually, as OPCs can also ensheathe nanofibers, imaging from the base to the tip of the pillars would allow for the quantification of rings made by OPCs and oligodendrocytes (Fig. 1e). Additionally, we engineered the pillars in a conical shape, allowing for visualization and resolution of concentric membrane wrapping along the entire length of the pillar from a single two-dimensional image (Fig. 1f). By measuring the dimensions of the MBP-positive membrane (base and tip diameter) from a compressed *z*-stack image, the length of the myelin-like segment can be interpolated from the dimensions of the pillar (Fig. 1d,f). We designed and optimized each pillar with a larger base diameter (50 μm) that tapers to the tip (2 μm) and is 25 μm in height (Fig. 1d). Essentially, individual pillars represent minimally permissive structures (length and diameter) that were previously determined by studies with nanofibers[18]. Each pillar is spaced at 50-μm intervals to allow for a reasonable number of oligodendroglia to adhere between the pillars (Fig. 1g) and to prevent membrane wrapping of multiple pillars from a single oligodendrocyte.

Oligodendrocytes cocultured with micropillars interacted with and ensheathed the pillars (Fig. 1g). Whereas multiple OPCs interacted with single pillars, we observed by scanning electron microscopy (SEM) that oligodendrocytes typically paired with a single pillar (Fig. 1g). After 5 d in culture, both OPCs (platelet-derived growth factor receptor-α (PDGFRα)-positive) and oligodendrocytes (MBP-positive) formed concentric rings around the pillars (Fig. 2a). We acquired a 10-μm compressed *z*-stack image of an oligodendrocyte and neighboring OPC that clearly illustrates that the oligodendrocyte wraps the pillar concentrically, whereas the OPC only partially ensheathes the pillar with an incomplete ring (Fig. 2b). This is consistent with previous findings illustrating ensheathment of nanofibers by OPCs and concentric wrapping by oligodendrocytes[18,19]. In addition, the MBP-positive membrane surrounding the pillar is thicker than the PDGFRα-positive membrane, suggesting that the wrapping by oligodendrocytes spreads along the length of the pillar.

Further examination of a 20-μm compressed *z*-stack image illustrates an oligodendrocyte wrapping an entire micropillar from top view, side view or from a 30°-tilted side-view image. Simple measurements of the base and tip diameters from the compressed *z*-stack image (Fig. 2c) permitted the resolution of the membrane extent and length of wrapping from a single two-dimensional image. Upon higher-magnification SEM imaging, we detected concentric membrane wrapping along the entire length of the pillar (Fig. 2d) and observed multiple layers of membrane near the tip of the pillar indicative of myelination (Fig. 2e). This is consistent with the myelin-like segments previously identified along the nanofibers. Nevertheless, the concentric wrapping identified around the pillars demonstrates the utility of the micropillars as a scaffold for membrane wrapping that is detectable in a high-throughput assay.

High-throughput screening for differentiation and myelination

The flexibility in the design of micropillars guarantees consistent uniformity in the experimental design, and any effects from compounds tested can be attributed solely to direct influences on oligodendroglia without effects from neurons. Currently, the arrays are designed as 5.0-mm^2-square chips bonded to the base of a 96-well bottomless plate. Approximately 10,000 micropillars are fabricated in each array, and 40,000 total OPCs are plated into each well. The number of OPCs were titrated and dispersed on to the micropillars to optimize for occupancy and reduce clustering of the cells. Additionally, the current density allows for analysis of effects on proliferation of OPCs and provides the sufficient range and space for detection.

The OPCs are seeded into the wells, allowed to settle and adhere for 48 h before the addition of screening compounds. Cells are cultured for 3 d with compounds at an initial concentration of 1 μM before fixation and immunostaining for MBP and PDGFRα. The 96-well plates are imaged on a motorized stage using a Zeiss LSM 700 confocal microscope and quantified by the Zen software. Upon initiating a screen of 1,000 bioactive molecules (Selleckchem), the effects of the compounds are quantified based on the average number of PDGFRα- and MBP-positive rings. These are acquired from four random 100-micropillar–containing fields from each individual array performed in triplicate. The data are plotted and grouped for proliferation and differentiation into four quadrants based on known positive control compounds (Fig. 3a). On average, the control wells display approximately 50% OPC rings and 10% oligodendrocyte rings. This is represented at the intersection of the green and red lines that indicate the extent of the error bars associated with the control measurements. In our work, addition of PDGF, a potent mitogen for OPCs, resulted in an increase in the number of PDGFRα-positive rings and a concomitant decrease in MBP-positive rings (Fig. 3a). This finding is consistent with the known role of PDGF as a mitogenic factor for OPCs that inhibits differentiation indirectly by promoting proliferation. As expected, addition of thyroid hormone (T3) and the tankyrase inhibitor XAV939 (ref. 20), compounds that promote differentiation and myelination, resulted in an increase in the number of MBP-positive rings and depletion of PDGFRα-positive rings (Fig. 3a). These findings are consistent with previously reported observations and validate the effectiveness of BIMA as a screening platform for oligodendrocyte differentiation and myelination.

Identification of antimuscarinic compounds

Upon completion of the screen, the majority of compounds tested were not found to have substantial effects on proliferation or differentiation of OPCs but instead caused a decrease in both PDGFRα- and MBP-positive rings. This finding suggests that multiple pathways and receptor ligands are necessary for OPC and oligodendrocyte survival and adhesion *in vitro* and that the decrease in oligodendroglial cells may be attributed to the toxicity of the limited concentrations of compounds tested (1 μM). In either case, future screening efforts and analysis of the compounds should reveal the direct or indirect effects on the decrease in the PDGFRα- and MBP-positive rings. Consistent with the fact that differentiation and proliferation are mutually exclusive processes, we identified clusters of compounds that promoted either proliferation or differentiation but not both (Fig. 3a). In order to determine the effectiveness of our approach, we examined the cluster of compounds that were most potent in the generation of MBP-positive rings with a concomitant decrease in PDGFRα-positive rings. We identified a cluster of eight FDA-approved antimuscarinic compounds that significantly enhanced oligodendrocyte differentiation and membrane wrapping (Fig. 3f). This cluster included the compounds atropine, ipratropium, oxybutynin, trospium, tiotropium, quetiapine, benzatropine and clemastine, also known as Tavist. Clemastine is a widely available first-generation antihistamine with a favorable safety profile for use. It is used primarily for symptomatic treatment of allergies and also exhibits antimuscarinic properties. We found that it greatly enhanced oligodendrocyte differentiation and wrapping (red rings) of micropillars, even when compared to the thyroid hormone T3 (Fig. 3b–f). In order to validate the cluster of molecules identified by BIMA, we analyzed the effects of the individual compounds on purified OPCs cultured in isolation (Fig. 4a–e and Supplementary Fig. 1), as well as on OPCs cocultured with purified dorsal root ganglion (DRG) neurons[21] (Fig. 4f–j).

Clemastine and benzatropine are FDA-approved compounds that cross the blood-brain barrier, and they were also the most effective in enhancing differentiation and myelination of oligodendrocytes (Fig. 4). To determine whether clemastine and benzatropine represent effective candidates for remyelination, we examined the dose-response relationship between clemastine or benzatropine administration and OPC differentiation (Supplementary Fig. 1g). Both compounds were most effective at 500 nM but promoted differentiation at as low as 10 nM. Consistent with findings from BIMA, the addition of clemastine, benzatropine or T3 significantly promoted differentiation and myelination without altering the number of oligodendroglial cells (Fig. 4f–j). Although screening these compounds using BIMA clearly illustrates the differences in efficacy between clemastine, benzatropine and T3, the effects observed using cocultures were less notable. This observation is due to the fact that oligodendrocytes form elaborate overlapping processes and can form numerous myelin internodes in cocultures, saturating the range of detection of the MBP-positive signal and thereby decreasing the resolution for quantifying changes between compounds. As each oligodendrocyte is paired to a single micropillar, the dynamic range for the detection of MBP rings is far greater than that for OPCs and allows for a more robust and linear analysis when screening compounds. Notably, these findings identify a cluster of FDA-approved compounds with the potential to promote repair in multiple sclerosis. Additionally, the ability to quantify a functional readout for differentiation and membrane wrapping by

oligodendrocytes represents a new opportunity to uncouple the contribution of active inductive cues on myelination from effects based on axon diameter alone.

Clemastine promotes remyelination *in vivo*

To determine whether clemastine represents an effective candidate for remyelination, we induced toxic injury in the white matter tracts of the spinal cord from adult mice and assessed the rate and extent of remyelination. We induced demyelination by injecting lysoleci-thin into the dorsal funiculus and ventrolateral white matter of adult mouse spinal cords (Fig. 5a)[20,22,23]. Essential to this demyelinating model is the timeline for repair, comprising active demyelination 1–3 days post lesion (d.p.l.), OPC recruitment (3–7 (d.p.l.), peaking at 5 d.p.l.), oligodendrocyte differentiation (7–10 d.p.l.) and active remy-elination (14–21 d.p.l.)[20,22–24]. On the basis of our previous findings, we analyzed oligodendrocyte differentiation at 7 and 14 d.p.l. and remyelination at 14 d.p.l. by electron microscopy (Fig. 5).

As clemastine has few adverse side effects, it represents a likely candidate for human remyelination trials. Therefore, we administered clemastine via oral gavage to adult mice at a concentration of 10 mg per kg body weight per day before initiating lysolecithin injections. *plp in situ* hybridization detected significantly more *plp*-positive oligodendrocytes in the lesion at 7 and 14 d.p.l. when compared to litter-mate controls (Fig. 5b,e). In addition, both *Cnp1 in situ* hybridization (Fig. 5c) and MBP immunostaining (Fig. 5d) of the lesions revealed enhanced differentiation of oligodendrocytes following the administration of clemastine at 14 d.p.l. Upon analysis of electron micrographs at 14 d.p.l., we found that the kinetics of remyelination were markedly accelerated in the lesions, with a corresponding decrease in the g-ratios (Fig. 5f–h), which represent myelin thickness with respect to axon size (ratio of axon diameter to the total fiber diameter). It is noteworthy that 29% of the axons detected were unmyelinated in the control lesions, whereas only 9% of the axons remained unmyelinated in the clemastine-treated mice (Fig. 5f). These findings further support the conclusion that clemastine greatly promotes differentiation and accelerates the kinetics of remyelination after a demyelinating insult.

DISCUSSION

High-throughput screening for myelin repair is problematic, as compact wrapping of oligodendrocyte membrane requires the presence of neuronal axons. Although *in vivo* screening of compounds using larval zebrafish[25,26] and *in vitro* screening using purified neuronal-oligodendroglial cocultures[21] have proven to be effective approaches, current methods do not resolve cell-autonomous and off-target effects, lack automated detection and quantification and are not well suited for high-throughput formats. Nevertheless, screenings with larval zebrafish and neuronal-oligodendroglial cocultures remain powerful tools that may be better suited for validation and secondary screening of compounds. Here we describe a binary indicant for myelination using micropillar arrays, which we named BIMA. Engineered with conical dimensions, micropillars permit resolution of the extent and length of membrane wrapping from a single two-dimensional image. The platform is currently formatted in 96-well plates and has also been designed to fit the 384-well plate format.

Notably, the platform is not limited to screening in a minimally permissive environment but is also ideally suited to examine inhibitory components in the lesion environment. The micropillar arrays can be coated with various inhibitory substrates or membrane components and screened for compounds that overcome inhibition of differentiation and wrapping. Additionally, the micropillars are not limited to fixation of cells and immunostaining for OPC and oligodendrocyte markers but are highly adaptive to mouse oligodendroglia from fluorescence reporter mice and amenable to time-lapse imaging of differentiation and myelination (Supplementary Fig. 2a–d). Identical to the behavior of rat OPCs, mouse OPCs interact with micropillars and, upon differentiation into myelinating oligodendrocytes, can be visualized by a fluorescence reporter (Supplementary Fig. 2e). Together, our results show that BIMA represents an unbiased approach for high-throughput screening of therapeutic compounds that can be adapted for continuous time-lapse imaging and may provide insight into new pathways and receptors essential for oligodendroglial development and myelination.

Upon completion of an initial screening of 1,000 bioactive molecules, we identified a cluster of eight FDA-approved compounds with antimuscarinic properties that enhanced oligodendrocyte differentiation and membrane wrapping. Included in this cluster is clemastine, a compound that exhibits both antimuscarinic and antihistaminic properties. The fact that five specific histamine receptor antagonists in the library do not display similar effects on oligodendroglia (data not shown) suggests that clemastine promotes oligodendrocyte differentiation and myelination via an off-target effect, namely, by blocking the muscarinic receptor. In line with this hypothesis, six muscarinic antagonists out of the cluster exhibited similar effects on oligodendroglia (Supplementary Fig. 1b–d). Previous reports confirm that muscarinic receptors are indeed expressed by oligodendroglial cells and may modulate OPC survival, proliferation and differentiation[27]. Clemastine represents the most effective compound among the cluster in promoting differentiation and myelination of oligodendroglia. Also, because clemastine penetrates the blood-brain barrier efficiently and has a favorable safety profile, it represents a promising candidate for multiple sclerosis therapy. We would be remiss if we did not mention that quetiapine, also known as Seroquel, is another FDA-approved compound that exhibits antimuscarinic properties and enhances oligodendrocyte differentiation and wrapping, albeit to a lesser extent than clemastine (Supplementary Fig. 1e,f). Whether quetiapine promotes oligodendrocyte differentiation and myelination by blocking muscarinic receptors is currently undetermined, as the class of atypical antipsychotics is highly nonspecific and may act on numerous receptors and pathways. Nevertheless, our studies illustrate that oral treatment with quetiapine is effective in promoting remyelination after lysolecithin demyelination (Supplementary Fig. 3). Taken together, the identification of the cluster of antimuscarinic compounds in our screen illustrates the proof of concept for BIMA as a high-throughput screening platform that represents a path to potential drug discovery for multiple sclerosis. We are confident that expansion of the screen to include larger chemical libraries, including more FDA-approved compounds and unique bioactive molecules, will result in the identification and development of rational therapeutics for repair in multiple sclerosis.

ONLINE METHODS

Fabrication of micropillar arrays

Photolithography methodology, routinely used in the semiconductor industry, is employed to fabricate micropillars within the target wells (Trianja Technologies). The starting substrate (fused silica) is coated with chrome and photoresist. The micro features are computer-generated and transferred to the photoresist layer by photolithographic technique. Subsequent pattern and etch steps are applied to complete the construction of micropillars. After the micro features are created, the chrome mask is removed and parts are divided from the substrate. Diced arrays are bonded to standard microwell plate frames for high-throughput analysis or singled out in subplate formats for assay development and optimization. This manufacturing method lends itself to high-volume production and is ready for scale-up.

Purification of oligodendrocyte precursor cells

Immunopanning purification of OPCs was performed as previously described[19]. Briefly, OPCs were purified from 7–9 postnatal rat or mouse brain cortices. Tissue culture dishes were incubated overnight with goat IgG and IgM secondary antibodies to mouse (Jackson Laboratories, cat. no.: 115-005-004) in 50 mM Tris-HCL, pH 9.5, at a final concentration of 10 μg ml^{-1}. Dishes were rinsed and incubated at room temperature with primary antibodies for Ran-2, GalC and O4 from hybridoma supernatants. Rodent brain hemispheres were diced and dissociated with papain (Worthington) at 37 °C. After trituration, cells were resuspended in a panning buffer (0.2% BSA in DPBS) and incubated at room temperature sequentially on three immunopanning dishes: Ran-2 and GalC were used for negative selection before positive selection with O4. OPCs were released from the final panning dish using 0.05% Trypsin (Invitrogen). OPCs are typically 95% pure after immunopanning, with a viability of 94%.

Screening compounds with BIMA

The 96 micropillar–well plates were coated with poly-L-lysine (100 μg ml^{-1}) for 1 h, washed twice with water and air dried. In each well, 40,000 rat OPC cells were seeded and maintained in chemically defined medium composed of DMEM (Invitrogen) supplemented with B27 (Invitrogen), N2 (Invitrogen), penicillin-streptomycin (Invitrogen), *N*-acetylcysteine (Sigma-Aldrich), forskolin (Sigma-Aldrich) and 12.5 ng ml^{-1} PDGF-AA (Peprotech) for 2 d before screening. Compounds (10 mM in DMSO, Chemical library, Selleckchem) were diluted to a final concentration of 1 μM in the absence of PDGF-AA and added to wells for 3 d before immunostaining. Each compound was tested in triplicate.

Immunostaining, image acquisition and quantification of PDGFRα- or MBP-positive rings on BIMA

Cultures were fixed with 4% PFA, dehydrated, permeabilized and blocked by incubation with 20% goat serum (Sigma-Aldrich) and 0.2% Triton X-100 (Sigma-Aldrich) in PBS. Differentiated oligodendrocytes and myelin membrane were detected with a rat monoclonal antibody to MBP (1:500, Millipore, Cat: MAB395), and OPCs were detected with a rabbit

monoclonal antibody to PDGFRα (1:8,000, gift from W.B. Stallcup)[18,19]. In the case of cocultures, neurons were detected with a mouse monoclonal antibody to neurofilament (NF) (1:200, Covance, Cat:SMI-32R). The Alexa Fluor 488, 594 and 647 IgG secondary antibodies against rat rabbit and mouse (1:1,000, Invitrogen) were used for fluorescence detection. Cell nuclei were identified with DAPI (Vector Labs). Fluorescent images from cultured oligodendroglia and cocultures were collected on a Zeiss Axio Imager Z1 fluorescence microscope with the excitation wavelengths appropriate for Alexa Fluor 488 (488 nm), 596 (568 nm), 647 (628 nm) or DAPI (380 nm). Image acquisition on BIMA (PDGFRα and MBP rings) was scanned using the Zeiss LSM-700 confocal microscope. Images from the screen were acquired at the *z*-position at 10–15 mm below the tip of the pillar. For statistical analysis, at least three representative fields (100 micropillars) were randomly acquired from each of the wells. Detection and quantification of the rings were performed using the Zen software (Zeiss) and the Image-Pro Plus software 5.0 (Media Cybernetics, Silver Spring, MD, USA).

Preparation of samples for scanning electron microscopy

All samples were fixed in 4% PFA stained with 1% osmium tetroxide for 1 h at 4 °C, counterstained with 1% uranyl acetate overnight and then dehydrated through ascending ethanol solutions (50, 70, 95 and 100% ETOH). After thorough drying, the samples were carefully mounted on an aluminum stub. Samples were then introduced into the chamber of the sputter coater and coated with a very thin film of gold before SEM examination (SEM analysis and image acquisition was performed at the University of Texas, Arlington).

Oligodendrocyte precursor cell–dorsal root ganglion cocultures

OPC-DRG cocultures were prepared as previously described[19]. Briefly, DRG neurons from E15 Sprague-Dawley rats were dissociated, plated (150,000 cells per 25 mm cover glass) and purified on collagen-coated coverslips in the presence of 100 ng ml^{-1} NGF (AbD Serotec). Neurons were maintained for 3 weeks and washed with DMEM (Invitrogen) extensively to remove any residual NGF before seeding OPCs. Cocultures were grown in chemically defined medium composed of DMEM (Invitrogen) supplemented with B27 (Invitrogen), N2 (Invitrogen), penicillin-streptomycin (Invitrogen), *N*-acetyl-cysteine (Sigma-Aldrich) and forskolin (Sigma-Aldrich).

Lysolecithin-induced demyelination in the spinal cord

Demyelinated lesions were induced in the dorsal funiculus and the ventrolateral white matter regions of the spinal cord of 8-week-old compound-treated and vehicle-treated female C57BL/6 mice as previously described[23]. Briefly, the animals were anesthetized with isofluorane and buprenorphine, and the spinal cords were exposed at level T12/13. 0.5 μL of 1% lysolecithin (L-α-lysophosphatidylcholine) was administered with a Hamilton needle for each lesion site. Six control mice and six mice orally treated with clemastine (10 mg kg^{-1} body weight) or quetiapine (5 mg kg^{-1} body weight) were injected and analyzed at 7 and 14 d.p.l.

Electron microscope analysis of remyelination

As previously described[23], mice were anesthetized and perfused transcardially with 4% glutaraldehyde at 14 d.p.l., and the spinal cord samples were postfixed overnight. Samples were stained with osmium tetroxide overnight and dehydrated in a series of ethanol dehydration treatments. Embedding was performed in TAAB resin. Sections were cut at 1-μm intervals and stained with toluidine blue for identifying lesion sites. 200 axons within lesion sites were examined using electron microscopy, and g-ratios were calculated as the diameter of the axon divided by the diameter of the axon and the surrounding myelin sheath.

Transgenic mice

All mice examined in this study were handled in accordance with the approval of the University of California San Francisco Administrative Panel on Laboratory Animal Care. The *plp*-CreER(T2) mice (The Jackson Laboratory) were bred to the tdTomato/EGFP line (The Jackson Laboratory) to generate *plp*-CreER(T2); tdTomato/EGFP littermate offspring. To induce the expression of EGFP in myelinating oligodendrocytes *in vitro*, cultures were treated with 4-hydroxytamoxifen (1 μM ml^{-1}) for 48 h before analysis.

Statistical analyses

Statistical analyses were performed using two-tailed Student's *t*-test to determine statistical significance that is expressed as $*P < 0.05$ and $**P < 0.01$ compared with control cultures or control mice without compound treatment (vehicle). The investigators were blinded to allocation of compounds during the high-throughput screening until the final statistical analysis. Sex- and age-matched C57BL/6 mice were randomly allocated to either control or treatment group for the lysolecithin experiments. No statistical method was used to predetermine sample size.

Supplementary Material

Refer to Web version on PubMed Central for supplementary material.

ACKNOWLEDGMENTS

We thank the Multiple Sclerosis Research Group at the University of California, San Francisco (UCSF) for support, advice and insightful discussions. This work was supported by the US National Multiple Sclerosis Society Harry Weaver Neuroscience Scholar Award (JF 2142-A2/T), UCSF CTSI Catalyst Award for Innovation, gifts from friends of the Multiple Sclerosis Research Group at UCSF and the Joint Research Fund for Overseas Chinese Young Scholars (NSCF, 31228011). The rabbit monoclonal antibody to PDGFRα was a gift from W.B. Stallcup (Sanford Burnham Medical Research Institute).

References

1. Franklin RJM. Why does remyelination fail in multiple sclerosis? Nat. Rev. Neurosci. 2002; 3:705–714. [PubMed: 12209119]
2. Keirstead HS, Blakemore W. Identification of post-mitotic oligodendrocytes incapable of remyelination within the demyelinated adult spinal cord. J. Neuropathol. Exp. Neurol. 1997; 56:1191–1201. [PubMed: 9370229]
3. Keirstead HS, Levine JM, Blakemore WF. Response of the oligodendrocyte progenitor cell population (defined by NG2 labelling) to demyelination of the adult spinal cord. Glia. 1998; 22:161–170. [PubMed: 9537836]

4. Scolding N, et al. Oligodendrocyte progenitors are present in the normal adult human CNS and in the lesions of multiple sclerosis. Brain. 1998; 121:2221–2228. [PubMed: 9874475]
5. Wolswijk G. Chronic stage multiple sclerosis lesions contain a relatively quiescent population of oligodendrocyte precursor cells. J. Neurosci. 1998; 18:601–609. [PubMed: 9425002]
6. Chang A, Nishiyama A, Peterson J, Prineas J, Trapp BD. NG2-positive oligodendrocyte progenitor cells in adult human brain and multiple sclerosis lesions. J. Neurosci. 2000; 20:6404–6412. [PubMed: 10964946]
7. Shi J, Marinovich A, Barres BA. Purification and characterization of adult oligodendrocyte precursor cells from the rat optic nerve. J. Neurosci. 1998; 18:4627–4636. [PubMed: 9614237]
8. Tang DG, Tokumoto YM, Raff MC. Long-term culture of purified postnatal oligodendrocyte precursor cells. Evidence for an intrinsic maturation program that plays out over months. J. Cell Biol. 2000; 148:971–984. [PubMed: 10704447]
9. Zawadzka M, et al. CNS-resident glial progenitor/stem cells produce Schwann cells as well as oligodendrocytes during repair of CNS demyelination. Cell Stem Cell. 2010; 6:578–590. [PubMed: 20569695]
10. Wolswijk G, Noble M. Cooperation between PDGF and FGF converts slowly dividing O-2Aadult progenitor cells to rapidly dividing cells with characteristics of O-2Aperinatal progenitor cells. J. Cell Biol. 1992; 118:889–900. [PubMed: 1323567]
11. Woodruff RH, Fruttiger M, Richardson WD, Franklin RJM. Platelet-derived growth factor regulates oligodendrocyte progenitor numbers in adult CNS and their response following CNS demyelination. Mol. Cell. Neurosci. 2004; 25:252–262. [PubMed: 15019942]
12. Colello RJ, Pott U. Signals that initiate myelination in the developing mammalian nervous system. Mol. Neurobiol. 1997; 15:83–100. [PubMed: 9396006]
13. Friede RL. Control of myelin formation by axon caliber (with a model of the control mechanism). J. Comp. Neurol. 1972; 144:233–252. [PubMed: 5029134]
14. Voyvodic JT. Target size regulates calibre and myelination of sympathetic axons. Nature. 1989; 342:430–433. [PubMed: 2586612]
15. Michailov GV, et al. Axonal neuregulin-1 regulates myelin sheath thickness. Science. 2004; 304:700–703. [PubMed: 15044753]
16. Taveggia C, et al. Neuregulin-1 type III determines the ensheathment fate of axons. Neuron. 2005; 47:681–694. [PubMed: 16129398]
17. Rosenberg SS, Kelland EE, Tokar E, De la Torre AR, Chan JR. The geometric and spatial constraints of the microenvironment induce oligodendrocyte differentiation. Proc. Natl. Acad. Sci. USA. 2008; 105:14662–14667. [PubMed: 18787118]
18. Lee S, et al. A culture system to study oligodendrocyte myelination processes using engineered nanofibers. Nat. Methods. 2012; 9:917–922. [PubMed: 22796663]
19. Lee S, Chong SYC, Tuck SJ, Corey JM, Chan JR. A rapid and reproducible assay for modeling myelination by oligodendrocytes using engineered nanofibers. Nat. Protoc. 2013; 8:771–782. [PubMed: 23589937]
20. Fancy SPJ, et al. Axin2 as regulatory and therapeutic target in newborn brain injury and remyelination. Nat. Neurosci. 2011; 14:1009–1016. [PubMed: 21706018]
21. Chan JR, et al. NGF controls axonal receptivity to myelination by Schwann cells or oligodendrocytes. Neuron. 2004; 43:183–191. [PubMed: 15260955]
22. Fancy SPJ, et al. Dysregulation of the Wnt pathway inhibits timely myelination and remyelination in the mammalian CNS. Genes Dev. 2009; 23:1571–1585. [PubMed: 19515974]
23. Chong SYC, et al. Neurite outgrowth inhibitor Nogo-A establishes spatial segregation and extent of oligodendrocyte myelination. Proc. Natl. Acad. Sci. USA. 2012; 109:1299–1304. [PubMed: 22160722]
24. Etxeberria A, Mangin JM, Aguirre A, Gallo V. Adult-born SVZ progenitors receive transient synapses during remyelination in corpus callosum. Nat. Neurosci. 2010; 13:287–289. [PubMed: 20173746]
25. Buckley CE, Goldsmith P, Franklin RJM. Zebrafish myelination: a transparent model for remyelination? Dis. Model. Mech. 2008; 1:221–228. [PubMed: 19093028]

26. Buckley CE, et al. Drug reprofiling using zebrafish identifies novel compounds with potential pro-myelination effects. Neuropharmacology. 2010; 59:149–159. [PubMed: 20450924]

27. De Angelis F, Bernardo A, Magnaghi V, Minghetti L, Tata AM. Muscarinic receptor subtypes as potential targets to modulate oligodendrocyte progenitor survival, proliferation, and differentiation. Dev. Neurobiol. 2012; 72:713–728. [PubMed: 21913336]

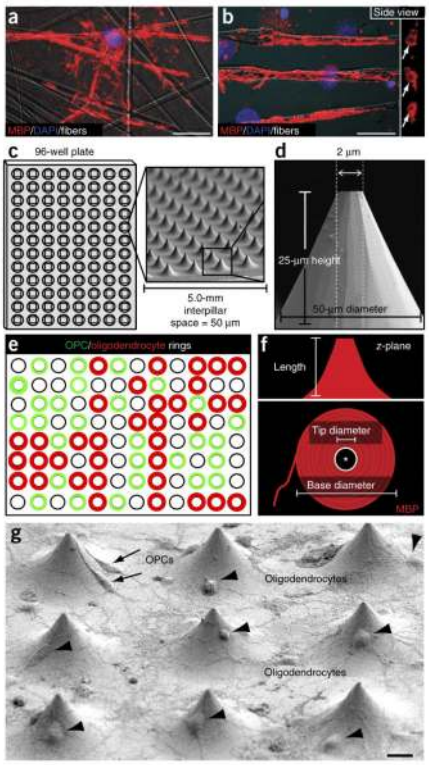

Figure 1.

Conception and fabrication of micropillar arrays for modeling myelination. (**a**) An oligodendrocyte wrapping nanofibers, visualized by MBP immunostaining. Scale bar, 20 μm. (**b**) Compressed *z*-stack image of oligodendrocytes wrapping nanofibers, visualized from the side and detected as 'rings' of myelin membrane (arrows, MBP-positive staining). Scale bar, 10 μm. (**c,d**) Conical micropillars, fabricated from fused silica and patterned for bonding into 96-well bottomless plates, imaged by SEM; interpillar distances and the physical dimensions of the pillars are also shown. (**e**) Illustration of the concept for micropillar arrays as a binary indicant for membrane wrapping. Using an inverted confocal microscope, the pillars can be imaged from the bottom of the plate, and OPC and oligodendrocyte membrane wrapping can be visualized and quantified. (**f**) Schematic diagram of a hypothesized compressed *z*-stack two-dimensional image of an oligodendrocyte wrapping a micropillar. Conceptually, a single high-resolution fluorescence image will allow for the measurement of the tip diameter and base diameter of membrane wrapping, as well as the corresponding extent and length in the *z*-plane. (**g**) Low-field SEM image of oligodendroglia interacting with and wrapping micropillars. Arrows show multiple OPCs interacting with single pillars, and arrowheads show oligodendrocytes paired with a single pillar. Scale bar, 10 μm.

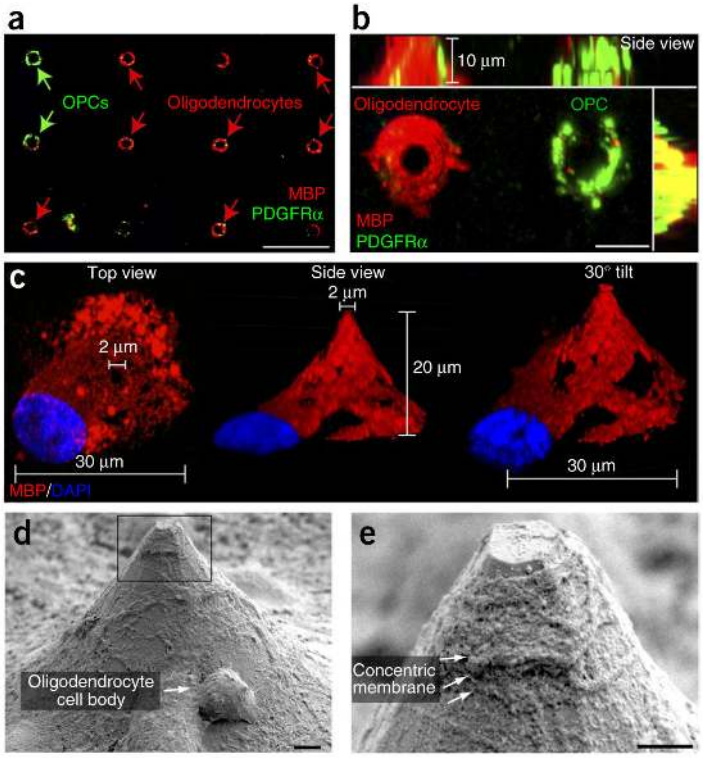

Figure 2.

BIMA. (**a**) Oligodendroglial cells interacting with the micropillars, detected by fluorescence confocal microscopy as green (PDGFRα-positive OPCs) or red (MBP-positive oligodendrocyte) rings. Scale bar, 25 μm. (**b**) High-magnification image of a 10-μm compressed *z*-stack image of an oligodendrocyte and a neighboring OPC. Scale bar, 10 μm. (**c**) A single oligodendrocyte XView image and with a 30° tilt from the side view. (**d**) SEM image of a single oligodendrocyte wrapping a micropillar. The arrow indicates an oligodendrocyte cell body. Scale bar, 1 μm. (**e**) High-resolution SEM image of the corresponding inset box in **d** illustrating multiple concentric layers of membrane made by the oligodendrocyte (as indicated by the arrows). Scale bar, 1 μm.

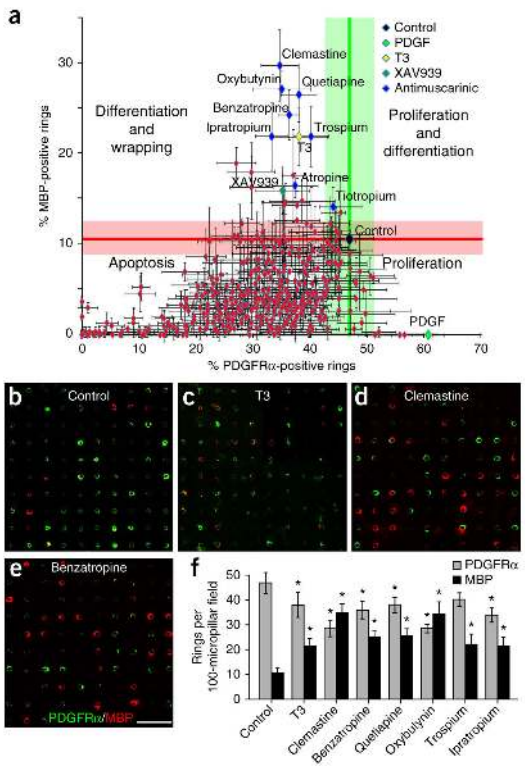

Figure 3.

High-throughput screening of bioactive compounds for differentiation and membrane wrapping identifies a cluster of antimuscarinic compounds. (**a**) Approximately 500 compounds were plotted based on the percentage of MBP-positive and PDGFRα-positive rings. Each compound was quantified and averaged based on four 100-micropillar fields from each array performed in triplicate. Based on the control arrays and known samples (PDGF, T3 and XAV939), compounds were categorized into four quadrants representing proliferation, apoptosis, differentiation and the combination of both proliferation and differentiation. The control (black diamond) is represented at the intersection of the green and red lines that indicate the average measurement of MBP-positive and PDGFRα-positive rings, as well as the extent of the s.e.m. associated with the control measurements. (**b**–**e**) Representative 100-micropillar fields immunostained for MBP (red) and PDGFRα (green) for control arrays (**b**), T3 (**c**), clemastine (**d**) and benzatropine (**e**). Scale bar, 100 μm. (**f**) Quantification for control, T3, clemastine, benzatropine, quetiapine, oxybutynin, trospium and ipratropium from the compound screen. Data are plotted as the number of MBP- or PDGFRα-positive rings in each field of 100 micropillars. Error bars represent mean ± s.e.m. $*P < 0.05$, significance based on Student's *t*-test with the respective controls.

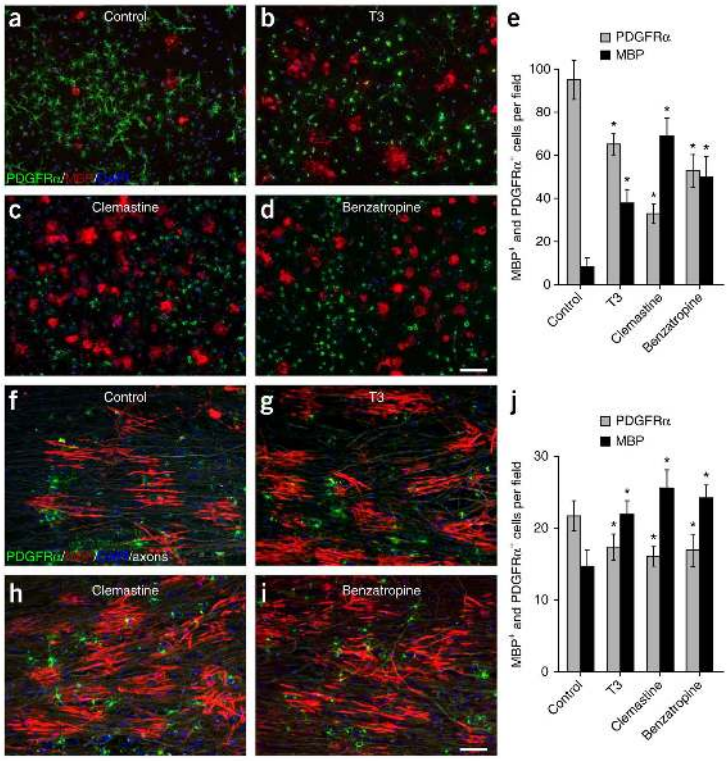

Figure 4.

Validation of clemastine and benzatropine with purified oligodendroglia cultured alone or with purified DRG neurons. (**a**–**d**) Control cultures (**a**) or cultures treated with T3 (**b**), clemastine (**c**) or benzatropine (**d**) for 3 d immunostained for MBP (red) and PDGFRα (green). Scale bar, 100 μm. (**f**–**i**) Control cocultures (**f**) or cultures treated with T3 (**g**), clemastine (**h**) or benzatropine (**i**) immunostained for MBP (red), PDGFRα (green) and neurofilament (white). Each of the single color images is displayed in a merged format with all three colors. Cell nuclei are identified by DAPI (blue). Scale bar, 50 μm. (**e**,**j**) Quantification of the percentages of MBP- and PDGFRα- positive cells from the purified OPC cultures (**e**) or DRG cocultures (**j**) in the presence of T3, clemastine or benzatropine. Error bars represent mean ± s.e.m., and all experiments were performed in triplicate. $*P < 0.05$, significance based on Student's *t*-test with the respective controls. $n = 3$ for all experiments.

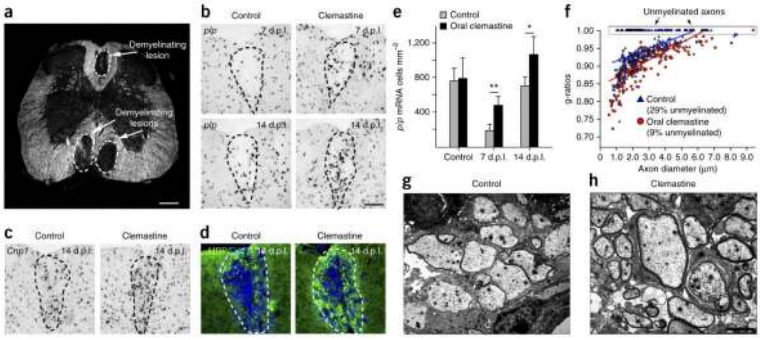

Figure 5.

Clemastine enhances the kinetics of remyelination and promotes remyelination in mice after gliotoxic injury with lysolecithin. (**a**) Dark-field micrograph of an adult mouse spinal cord illustrates focal demyelinated lesions in the dorsal funiculus and ventrolateral white matter. Scale bar, 300 μm. (**b**) Focal demyelinated lesions induced by injection of lysolecithin (n = 6) in mice treated with or without clemastine. *In situ* hybridization of *plp* in the lesions were examined after oral administration of clemastine at 7 and 14 days post lesion (d.p.l.). Scale bar, 100 μm. (**c**,**d**) Mice at 14 d.p.l. were subjected to *Cnp1 in situ* hybridization (**c**) and MBP staining (**d**) following the administration of clemastine and demyelination. Dashed lines demarcate lesion areas. Scale bar in **b** applies to **c** and **d**. (**e**) Quantification of *plp in situ* hybridization. Error bars represent mean ± s.d., and all experiments were performed in quadruplicate. *P = 0.05, **P = 0.009, significance based on Student's t-test. (**f**) Quantification of myelin sheath thickness and the proportion of myelinated and unmyelinated axons in control (blue) and clemastine-treated (red) mice at d.p.l. by g-ratio analysis. The scatterplot displays g-ratios of individual axons as a function of axonal diameter. All g-ratios were analyzed from transmission electron microscopy images. (**g**,**h**) Representative electron microscopy images for control (**g**) and clemastine-treated (**h**) mice at 14 d.p.l. Scale bar, 2 μm.